applied sciences

MDPI

Article

Multispectral Detection of *Planktothrix rubescens* Blooms in Volcanic Lakes Using Sentinel-2: Proof of Concept of a Newly Characterized Spectral Signature

Cristiano Ciccarelli [1,†], Mohammed Ajaoud [1,†], Milena Bruno [2], Valentina Messineo [2], Marco Casazza [3,*] and Massimiliano Lega [1,*]

[1] Department of Engineering, University of Naples Parthenope, Centro Direzionale di Napoli Isola C4, 80143 Naples, Italy; cristiano.ciccarelli@phds.uniparthenope.it (C.C.); mohammed.ajaoud@phds.uniparthenope.it (M.A.)
[2] Department of Infectious Diseases, Istituto Superiore di Sanità, Viale Regina Elena 299, 00161 Rome, Italy; milena.bruno@iss.it (M.B.); valentina.messineo@iss.it (V.M.)
[3] Department of Medicine, Surgery and Dentistry Scuola Medica Salernitana, University of Salerno, 84081 Baronissi, Italy
* Correspondence: mcasazza@unisa.it (M.C.); massimiliano.lega@uniparthenope.it (M.L.); Tel.: +39-0815476582 (M.L.)
† These authors contributed equally to this work.

Featured Application

The proposed Sentinel-2 multispectral signature can potentially be used as a screening tool for the operational monitoring of *Planktothrix rubescens*-dominated blooms in lakes and reservoirs. Automated flagging of the characteristic blue-to-green spectral pattern could support targeted field sampling and laboratory analyses, providing a cost-effective complementary layer for early-warning workflows for the management of drinking water and recreational water, pending validation across broader datasets and lake types.

Abstract

Cyanobacterial harmful algal blooms threaten freshwater quality, ecosystem stability, and public health, creating a need for spatially extensive monitoring tools that complement in situ observations. This study evaluates whether Sentinel-2 multispectral imagery can be used to identify a recurrent spectral pattern associated with *Planktothrix rubescens* blooms in two volcanic lakes in Central Italy (Albano and Vico). Sentinel-2 Level-1C data were processed with C2RCC to retrieve water-leaving reflectance and compared with microscopy-based observations across 13 acquisition dates (eight bloom and five no-bloom events). At the event level, bloom and no-bloom conditions were spectrally distinguishable. Six of eight bloom spectra showed a green-band peak at 560 nm and a pronounced increase from blue (443–490 nm) to green wavelengths. The B3/B1 ratio was 3.04 under bloom conditions versus 1.12 under no-bloom conditions, while B3/B2 was 1.77 versus 0.76 (both $p < 0.05$). Within bloom events, the blue-to-green ratio was not significantly correlated with cell density, indicating that the pattern is more suitable for bloom detection than abundance estimation. The recurrent pattern was formalized as a simple Type A criterion and further assessed using cosine similarity. These results support Sentinel-2 as a proof-of-concept screening tool for *P. rubescens*-dominated blooms, pending broader validation.

Keywords: CyanoHABS; environmental impact assessment; environmental monitoring; remote sensing; spectral signature

Check for updates

Academic Editor: Ramaraj Boopathy

Received: 20 July 2026
Revised: 24 September 2026
Accepted: 25 September 2026
Published: 28 September 2026

Copyright: © 2026 by the authors. Licensee MDPI, Basel, Switzerland. This article is an open access article distributed under the terms and conditions of the Creative Commons Attribution (CC BY) license.

1. Introduction

In recent decades, cyanobacterial blooms have emerged as a critical issue for environmental and human health. This phenomenon is primarily driven by eutrophication from anthropogenic activities, which disrupts aquatic ecosystems and leads to imbalances in phytoplankton populations, favouring the dominance of cyanobacteria [1]. The resulting cyanotoxin production propagates through food webs, exerting toxic effects on animal and plant species, with potential impacts extending to human health [2]. Consequently, the implementation of rapid, widespread water monitoring and control systems is required to detect, monitor, and mitigate environmentally hazardous conditions, that could escalate into harmful bloom events.

With this respect, environmental monitoring of freshwater ecosystems is essential for detecting early warning signals of ecosystem degradation and for supporting water management decisions. However, traditional monitoring approaches, based solely on in situ sampling, while accurate, are limited in spatial coverage and temporal frequency, making them insufficient for capturing the dynamic nature of algal blooms. Meanwhile, satellite remote sensing offers a complementary perspective, enabling systematic observation of water bodies over larger areas. Nonetheless, its use, if not combined with other monitoring approaches, while potentially representing a gain in terms of early warning and larger spatial coverage, risks the loss of precious information in terms of spatial detail and observation frequencies. This is the reason behind the implementation of multi-level multi-parametric observation frameworks [3]. This type of approach can integrate different levels of observation, from remote and proximal sensing methods performed through the use of different satellite or aerial platforms, to in situ samplings that can be further elaborated in the laboratory. Both bottom-up (from in situ sampling to remote sensing) and top-down (from satellite to in situ sampling) approaches are possible, depending on the investigated context. However, to be effective, this framework requires not only a sufficient level of technological and operational integration, but also the implementation of analytical procedures to identify the signature of potentially harmful substances or processes. In the case of cyanobacteria, together with other water quality indicators, chlorophyll a (Chl-a) and phycocyanin spectral signatures are traditionally used for identifying the potential presence of blooming [4,5]. For example, the satellite platform Sentinel-2, part of the European Copernicus Program, provides suitable optical remote sensing data, with a spacetime resolution of 13 spectral channels, able to detect chlorophyll a (Chl-a) concentration and measure turbidity, which are important water quality indicators widely applied for inland water quality monitoring [6–8].

Among toxigenic cyanobacteria, whose presence can be detected through remote sensing techniques, *Planktothrix rubescens* is a filamentous freshwater species, frequently occurring in deep, thermally stratified lakes and reservoirs. Its efficient buoyancy regulation and its accessory photosynthetic pigments, particularly, phycoerythrin and phycocyanin, allow it to thrive under low-light conditions and to form dense populations in the metalimnion or upper hypolimnion, often resulting in a deep chlorophyll maximum [9,10]. Its development is influenced by nutrient availability, particularly, phosphorus, although persistent or recurrent blooms can also occur in mesotrophic and re-oligotrophicated lakes. Water-column stability, thermal stratification, and changes in seasonal mixing therefore play major roles in controlling its abundance. *P. rubescens* is of particular environmental and public health concern because toxigenic populations can produce several microcystin congeners, which may contaminate water resources and aquatic organisms and consequently represent a potential exposure risk for humans and wildlife [11]. Moreover, its tendency to develop dense subsurface layers represents an additional challenge for satellite-based monitoring, since optically detected surface conditions may not fully represent the abundance

of populations located deeper in the water column. In European lakes, *P. rubescens* is one of the most widespread toxin-producing cyanobacteria and is responsible for recurrent bloom events. In Italy, it is recognized as a winter specie, with blooms often extending from late autumn to mid-spring [12]. Its presence was first documented in Albano lake (Lazio region, Italy) in 1953 [13].

Using satellite imagery data from MODIS Terra, empirical relationships have been established to estimate the cell density of *P. rubescens*. However, satellite data alone were not sufficient to distinguish it reliably from other cyanobacterial taxa, highlighting the need for higher-resolution approaches [10]. Conversely, the effectiveness of a multi-scale integrated approach was demonstrated in Occhito lake, facilitating the creation of surface lake-wide maps illustrating the distribution of *P. rubescens* [14]. Nonetheless, a specific spectral signature for this cyanobacterium has not yet been defined in the literature. This is why this study aims to characterize the spectral response associated with *P. rubescens* blooms through the use of multispectral remote sensing techniques. The novelty of this approach consists in the detection of phycoerythrin (PE), determining the red pigmentation of *P. rubescens* [15], instead of other chlorophyll-based indices (such as Normalized Difference Vegetation Index, NDVI) for characterizing of green-algae-dominated waters. The reason behind this choice is that PE alters the optical response of these blooms compared with green-algae-dominated waters, so that maps derived from chlorophyll indices typically do not produce useful results [16]. Consequently, the present research focused on the search for the identification of characteristic spectral signature, based on the reflectance of materials across specific wavelengths, which are distinctive for each material and can therefore be used to identify the presence of such materials in different environmental contexts.

In this regard, the scientific literature on the spectral signature of cyanobacteria remains surprisingly limited, despite their ecological and environmental significance. The research on HABs is generally oriented towards a broad multispectral observation of water bodies, basically employing remote indices to locate cyanobacteria proxies, such as the concentration of Chl-a. Recent advancements in hyperspectral remote sensing have significantly improved our capacity to discriminate cyanobacterial genera based on detailed pigment absorption features [17,18]. However, the operational application of these findings for routine monitoring by environmental agencies is often constrained by the availability, cost, and complexity of hyperspectral data. In contrast, multispectral sensors, like Sentinel-2 MSI, offer free, frequent, and systematically acquired data, making them the current workhorse for operational water quality monitoring. Consequently, to bridge the gap between advanced hyperspectral discrimination and operational multispectral monitoring, this study proposes and tests a reproducible multispectral signature pattern associated with *P. rubescens*. In particular, we provide a statistically characterized spectral signature of *P. rubescens*-dominated blooms in volcanic lakes, employing operational satellite data. This work does not aim to replace hyperspectral techniques, but rather to adapt spectral signature analysis into a practical, operational tool for bloom detection through freely available multispectral data. This solution is able to provide valuable support for informed decisions in environmental management and to address a critical need in current harmful algal blooms (HABs) monitoring strategies.

2. Materials and Methods

2.1. Study Sites

Two Italian lakes, Albano and Vico lakes (Figure 1), both located in Lazio region (central Italy), were selected for this study. The Albano lake is a volcanic basin within a crater depression characterized by a perimeter of 12 km, a surface of 6 km^2, and a maximum depth of 175 m [19]. This lake is a hydrologically closed basin, receiving water mainly from

atmospheric precipitation and underwater springs. *P. rubescens* population dynamics in Albano lake show surface stratification with blooms in winter and metalimnic stratification during summer, peaking at depths of 25–30 m. However, there is an overall population decline of 80–86% from late April to early November. In spring, with frequent cold and rainy weather, the thermal stratification of the upper layers is sensitive to climatic fluctuations, occasionally leading to unusual rises in *P. rubescens* populations, resulting in surface scums even in April–May. Vico lake is another volcanic lake, located within a crater depression of the Cimino volcano complex. It has a surface area of 12.63 km^2, a perimeter of 17.71 km, and a maximum depth of 48.5 m. It is part of a Regional Wildlife Park and is designated as a wetland of international importance under the Ramsar Convention. The surrounding area features extensive hazel woods. Lake Vico serves as a drinking water reservoir for around 10,000 residents of Ronciglione and Caprarola and is a popular recreational area throughout the year. Both these lakes undergo a progressive eutrophication process, manifested through periodic *P. rubescens* blooming, particularly between winter and spring.

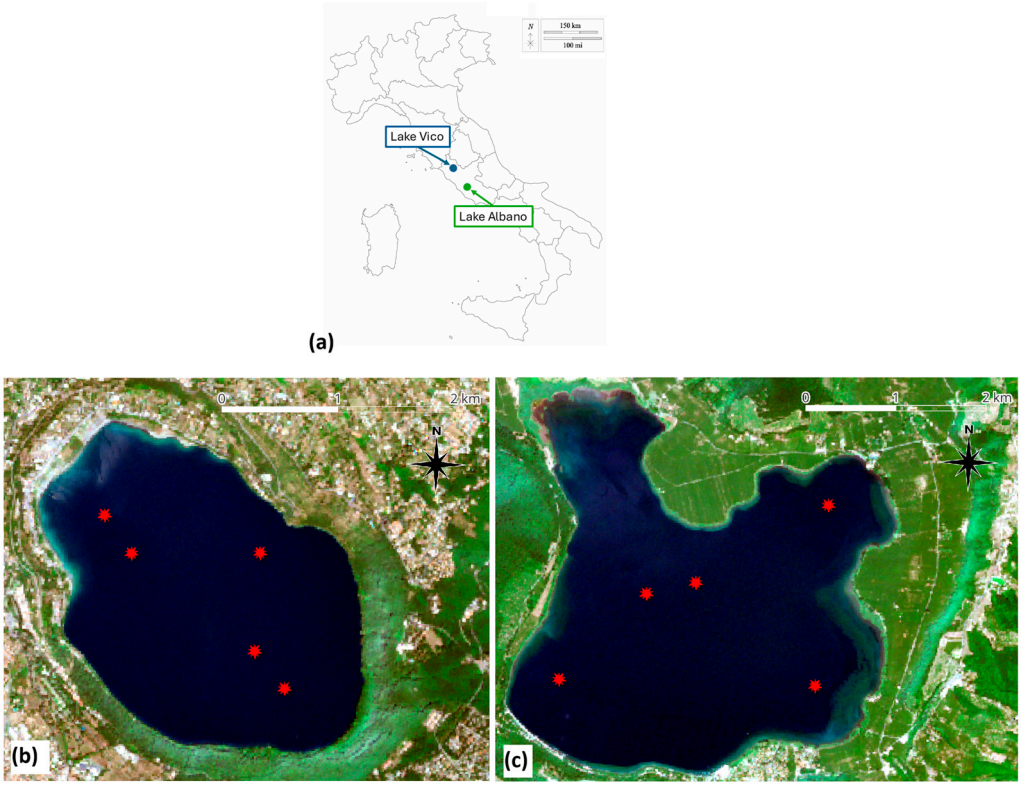

Figure 1. (**a**) Map of Italy, with position of Albano (green dot) and Vico (blue dot) lakes. (**b**) Aerial photo of Lake Albano collected in day 8 July 2025, as red stars the position of the five sampling stations (from upper left to down right: Molo, Castello, Hotel, Centro, Bosco). (**c**) Aerial photo of Lake Vico collected in day 8 July 2025, with positions of the five sampling stations (in clockwise order, starting from upper left: Baia Bella Venere, Emissario, Promontorio, Ultima Spiaggia, Centro Superficie). Both aerial photos were acquired from Copernicus Browser and are for cartographic reference only.

2.2. Data Sources and Methods

2.2.1. Sample Collection and Microscopic Observation

As shown in Figure 1, to have a ground sampling and validation of remotely sensed data, five sampling points were chosen in both Albano and Vico lakes, following a T-shape geometrical pattern, at a minimum distance of 50 m from the shore. A further sampling point was taken in the middle of the lake. Water samples for toxicological and biological analyses were collected monthly by filling 1 L Pyrex glass bottles 10–20 cm below the water

surface. Samples were stored in ice chests and transported to the laboratory for analysis. The in situ *P. rubescens* densities collected at 10–20 cm below the surface are consistent with the near-surface layer that dominates the water-leaving reflectance sensed by Sentinel-2.

Microscopic examination, Chl-*a* quantification, toxin extraction, and quantification were conducted in the laboratory. For microscopic observations, subsamples were analyzed within 48 h from the sampling, with a LABOVERT inverted microscope (Ernst Leitz Wetzlar GmbH, Wetzlar, Germany), following the traditional methods described in the literature [20,21], using 25 mL sedimentation chambers for phytoplankton identification and cell density. Chl-*a* content was measured in 90% acetone extracted samples, following the SCOR/UNESCO method [22], using a Lambda Bio spectrophotometer (25 UV/Vis spectrophotometer; PerkinElmer, Shelton, CT, USA).

The days for which satellite data were analyzed were chosen between the dates identified by the chemical analysis as bloom days or days without bloom events (referred as no-bloom days hereafter). Specifically, dates when microscopic analysis identified *P. rubescens* with non-zero sub-surface cell density were classified as bloom, while the dates when *P. rubescens* was absent were labelled as no-bloom. For context, superficial blooms of *P. rubescens* in these lakes are known to exceed the Italian tolerance limit of 5×10^6 cells/L set for surface scum. Sub-surface densities here reported are consistent with, though not directly comparable to, that surface-referenced threshold.

The selected days are presented in Table 1.

Table 1. List of selected bloom and no-bloom days for Lake Albano and Vico, here shown in chronological order.

Lake	Date
Albano	31 May 2018
Albano	15 June 2018
Vico	5 July 2018
Vico	26 October 2018
Vico	5 December 2018
Albano	12 December 2018
Vico	14 January 2019
Vico	13 February 2019
Albano	20 February 2019
Albano	22 March 2019
Vico	25 March 2019
Vico	24 May 2019
Vico	13 June 2019

2.2.2. Multispectral Satellite Images

We used data recorded from the Sentinel-2 satellite platform, two twin satellites both carrying a MultiSpectral Imager (MSI) (Airbus Defence and Space, Toulouse, France), often employed for chlorophyll and vegetation monitoring. The satellites fly the same orbit, but phased out of 180°, to achieve a revisit period of 5 days at the Equator.

The employed data were Sentinel-2 Level-1C (L1C) MSI data downloaded via the Copernicus Data Space Ecosystem. Sentinel-2 L1C products are distributed as granules (or tiles). These tiles consist of 100×100 km ^{2} ortho-images in UTM/WGS84 cartographic projected coordinate system representing top-of-atmosphere reflectance for 13 spectral bands (Table 2).

Table 2. The 13 bands observed by Sentinel-2/MSI, along with central wavelength, bandwidth, and resolution.

S-2 Band	Central Wavelength (nm)	Bandwidth (nm)	Resolution (m/px)
Band 1	443	20	60
Band 2	490	65	10
Band 3	560	35	10
Band 4	665	30	10
Band 5	705	15	20
Band 6	740	15	20
Band 7	783	20	20
Band 8	842	115	10
Band 8A	865	20	20
Band 9	945	20	60
Band 10	1375	30	60
Band 11	1610	90	20
Band 12	2190	180	20

Subsequently, the S-2 L1C data were processed on Sentinel Application Platform v13.0 (SNAP), the official toolbox software of the European Space Agency (ESA). The processor employed was the Case 2 Regional CoastColour (C2RCC) processor. This processor is specifically designed to process Case 2 waters (waters with a complex mixture of suspended matter, typically coastal and inner waters, in contrast to Case 1 waters, mainly oceanic ones).

The obtained processing output was the water-leaving reflectance values (ρ_w) of 8 Sentinel-2 bands, from Band 1 to Band 7 and Band 8A. The value ρ_w is calculated as $\pi \times \frac{L_w}{E_d}$, where L_w is the water-leaving radiance and E_d is the incident radiance.

2.2.3. Numerical Methods

To compare the shapes of the spectral signatures, min–max normalization was applied at pixel level prior to spectral averaging. As in the case of absolute value signatures, the mean normalized spectral signature was then calculated for each event (either bloom or no-bloom day). Min–max normalization is a commonly used method to normalize spectral data [23,24]. In this study, the eight-band reflectance spectrum of each pixel was rescaled to the [0, 1] interval, using the minimum and maximum of the entire spectrum (per-spectrum min–max normalization), computed as follows:

$$\tilde{x_b} = \frac{x_b - min_b x_b}{max_b x_b - min_b x_b} \quad (1)$$

where x_b represents the ρ_w value of a given pixel in a spectral band b, while $max_b x_b$ and $min_b x_b$ denote, respectively, the maximum and minimum ρ_w values across the eight bands of that same pixel. Thus, normalization is applied independently to each pixel, with the maximum and minimum values recalculated for every spectrum. For each event, the normalized spectra across the five ROIs were pooled and the mean normalized signature was computed over this pooled set of pixels. This per-spectrum normalization preserves the inter-band shape of each signature and removes only its absolute magnitude, isolating the spectral shape.

Differences between bloom and no-bloom conditions were assessed at the event level, treating each acquisition date as the statistical unit (8 bloom and 5 no-bloom days), to avoid the artificial replication that would arise from treating spatially autocorrelated pixels as independent samples. For each band, the mean bias error (MBE) was computed as the

difference between the mean normalized reflectance of bloom and no-bloom dates. The MBE formula is:

$$MBE = \frac{1}{n}\sum_{i=1}^{n}(x_i - y_i) \quad (2)$$

where x_i are the pixels normalized spectral signatures for bloom days, y_i the signatures for no-bloom days. Statistical significance was evaluated with the Mann–Whitney U test as the primary test, given the small sample size and the non-normal distribution of the data, while Welch's *t*-test was reported as a parametric cross-check, calculated as follows:

$$t = \frac{\bar{X}_1 - \bar{X}_2}{\sqrt{\frac{s_1^2}{n_1} + \frac{s_2^2}{n_2}}} \quad (3)$$

where $\bar{X}_1$ and $\bar{X}_2$ are the mean of the two samples, while s_1^2 and s_2^2 are the two sample variances related to n_1 and n_2 samples. In addition, band ratios were calculated with non-normalized mean signatures, comparing between conditions with the same event-level test. In this respect, we acknowledge that the limited number of dates reduces the statistical power, so this analysis is interpreted from a proof-of-concept perspective.

To explore whether the spectral response was quantitatively related to the in situ data, a Spearman correlation was computed between mean cell density and the non-normalized blue-to-green ratio (Band 3/Band 1) [25,26].

Once the presence of a difference between bloom days and no-bloom days was established, common behaviour between the spectral signatures of different blooms had to be verified. Firstly, a simple spectral classification, applying a method available in the literature [27], was adapted to our purpose, in order to look for recurrent features among bloom signatures. Most of these signatures share monotonic increase from blue to green bands. Hence, this trend was formalized as a reproducible criterion, here referred to as Type A. As already stated, this rule was derived observationally from the available bloom signatures, rather than obtained by optimizing a decision threshold. Thus, Type A can be viewed as a compact, qualitative descriptor of the observed pattern and as a potential building block for future operational classifiers, rather than as a trained or validated classification model. The classification algorithm generated and employed was as follows:

$$\begin{array}{c} if\ \frac{B2}{B1} > 1\ and\ \frac{B3}{B2} > 1 \rightarrow Type\ A \\ Otherwise \rightarrow Unknown \end{array} \quad (4)$$

To observe the similarity between different bloom signatures, cosine similarity (CS) calculation was performed [28,29]. CS is defined as the cosine of the angle between two vectors, taking a value of 1 if the vectors have identical orientation and 0 if they are orthogonal. In particular, CS was applied here to the first-order discrete spectral derivatives of absolute spectral signatures, to emphasize similarities in spectral shape while excluding the influence of absolute reflectance magnitude. Given an original spectral signature defined over n spectral bands (n = 8), the discrete spectral derivative vector is defined as follows:

$$\Delta\vec{p} = (p_2 - p_1,\ p_3 - p_2,\ \ldots,\ p_n - p_{n-1}) \quad (5)$$

resulting in a vector of dimension $n - 1$. Then, the CS was computed between pairs of derivative vectors, which lie in a $n - 1$-dimensional space, as follows:

$$K\left(\Delta\vec{p_i}, \Delta\vec{q_i}\right) = \frac{\Delta\vec{p_i} \cdot \Delta\vec{q_i}}{\left|\Delta\vec{p_i}\right|\left|\Delta\vec{q_i}\right|} \quad (6)$$

where $\Delta\vec{p} = (p_2 - p_1, \ldots, p_n - p_{n-1})$ and $\Delta\vec{q} = (q_2 - q_1, \ldots, q_n - q_{n-1})$ represent the discrete spectral derivatives of two bloom spectral signatures, with components corresponding to reflectance variations between adjacent spectral bands.

2.3. Workflow

The workflow to prepare and analyze the data followed a structured approach. The raw data were retrieved from Copernicus Dataspace Catalogue as granules. The tiles were processed through the Sentinel Applications Platform (SNAP) v13.0 software. Firstly, a resampling at 10 m/px (resolution of Bands 2, 3, 4 and 8) with bilinear interpolation was implemented for the data of all the bands required for the processing. Subsequently the Case 2 Regional CoastColour (C2RCC) processor was employed to process the multispectral images. This processor is specifically designed to process Case 2 waters. The tiles were processed through C2RCC, which returned the water-leaving reflectance of aquatic areas in the tiles and the relative flags. In particular, the C2RCC processor returns eight processed bands (Bands 1 to 7 and 8A) from the thirteen observed by Sentinel-2/MSI. Water-leaving reflectance is calculated as $\rho_w = \pi \times \frac{L_w}{E_d}$ where L_w is the water-leaving radiance and E_d is the incident radiance.

Once the tiles were processed, the data were filtered to obtain exclusively ρ_w values of the valid pixels, which were those inside the perimeter of the lakes and not affected by flags (such as clouds or algorithm failures). The perimeters were obtained by manually tracing the lakes shapes as shapefiles, and a 20 m buffer was additionally imposed in order to avoid coastal influence.

Finally, ROIs were established by drawing 5 px × 5 px squares around the pixels containing the ground sampling points, obtaining 50 × 50 m^2 ROIs.

3. Results

The in situ *P. rubescens* cell densities for the analyzed dates are reported in Table 3. For each day, the mean cell density values of *P. rubescens* (cell/mL) across the five sampling stations are presented. Bloom dates were characterized by sub-surface densities ranging from 3.5×10^5 to 1.3×10^7 cell/L, while no-bloom days showed absence or non-detection of the species, hence providing a direct, microscopy-based confirmation that the analysed bloom events had a strong presence of *P. rubescens*.

Table 3. List of selected bloom and no-bloom days for Lakes Albano and Vico, here shown in chronological order. For each day, the mean cell density values of *P. rubescens* (cell/mL) are included.

Lake	Date	Mean Cell Density (Cell/mL)	Condition
Albano	31 May 2018	0	No-bloom
Albano	15 June 2018	0	No-bloom
Vico	5 July 2018	0	No-bloom
Vico	26 October 2018	1175	Bloom
Vico	5 December 2018	1859	Bloom
Albano	12 December 2018	12,765	Bloom
Vico	14 January 2019	2171	Bloom
Vico	13 February 2019	2921	Bloom
Albano	20 February 2019	649	Bloom
Albano	22 March 2019	942	Bloom
Vico	25 March 2019	353	Bloom
Vico	24 May 2019	0	No-bloom
Vico	13 June 2019	0	No-bloom

Across all 13 dates (8 bloom and 5 no-bloom), the Spearman correlation was moderate and marginally significant ($\rho = 0.55$, $p = 0.05$), reflecting the contrast between bloom and no-bloom days. Within the eight bloom dates alone, no significant relationship emerged ($\rho = 0.12$, $p = 0.78$). Hence, cell density did not predict the steepness of the blue-to-green increasing trend, an effect partly driven by highest-density events with atypical spectral signature shapes. This indicates that the spectral signature was associated with the presence of a surface bloom, rather than with its cell density.

From the filtered data, it was possible to obtain a variety of different spectral signatures, relative to the different dates when the two lakes experienced blooming events. Figure 2 shows as an example the spectral signature of the 5 December 2018 bloom event in Vico lake. The different ROIs' spectral signatures are distinguished by colour. It can be seen that the different ROIs share strongly similar signatures, in terms of both shape and ρ_w magnitude observed across all the events.

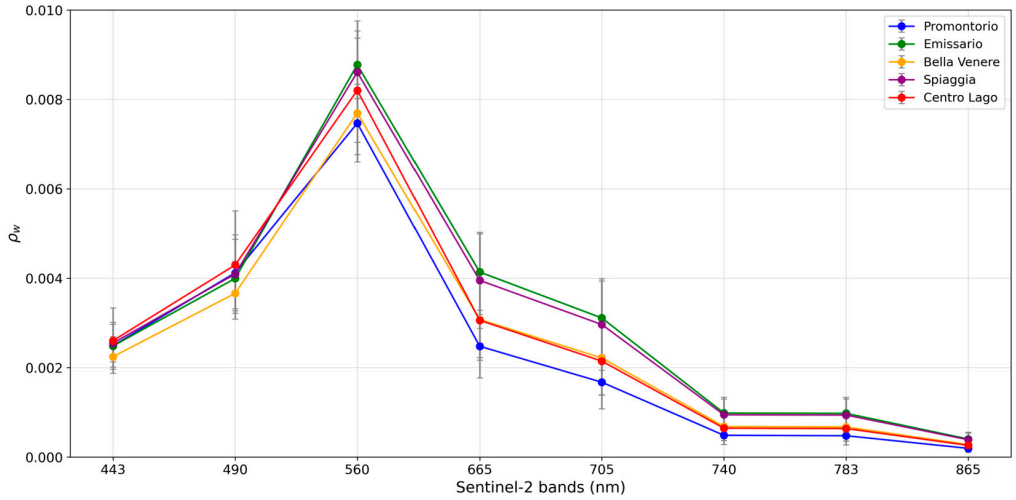

Figure 2. Mean spectral signatures of the five different ROIs (Promontorio in blue, Emissario in green, Bella Venere in yellow, Spiaggia in purple, and Centro Lago in red) for Lake Vico on the bloom day 5 December 2018.

The mean spectral signatures along all the ROIs pixels available for each date are shown in Figure 3. In these graphs, each spectral signature is distinguished through different line types and colours. The upper graph shows Albano lake signatures, while the second refers to the Vico lake signatures.

Some distinguishable key features are shared by the spectral signatures. All different spectra flatten from 740 nm (Band 6) to the end. Conversely, the peak falls either in the first/second or in the third band for all the signatures. In particular, the higher peak is at 490 nm (Band 2, blue), but most of the signatures have their peak at 560 nm (Band 3, green). It is also notable that the no-bloom signatures have the highest value for the peaks and the ρ_w for the first three bands is generally higher in these signatures. A strong difference in magnitude of the ρ_w values of the first band (443 nm) between no-bloom and most of the bloom signatures is evident, with the first ones showing strongly higher values.

After the min–max normalization, implemented to exclude the effects of ρ_w intensity in the analysis, the obtained daily mean spectral signatures are shown in Figure 4. Most of the spectral signatures (especially those of bloom days) exhibit a peak in the 560 nm band, with a decreasing trend that varies in steepness in the bands towards the infrared. Conversely, a smaller number of mean spectral signatures show a peak in the blue region (443 nm and 490 nm). This feature belongs especially to the no-bloom days at Albano Lake, which appear to have this distinguishably different feature. Lastly, it is notable that the

two no-bloom signatures for Vico lake that peak in the 560 band still exhibit a different increasing trend between 443 nm and 560, with values in the blue region closer to the peak value.

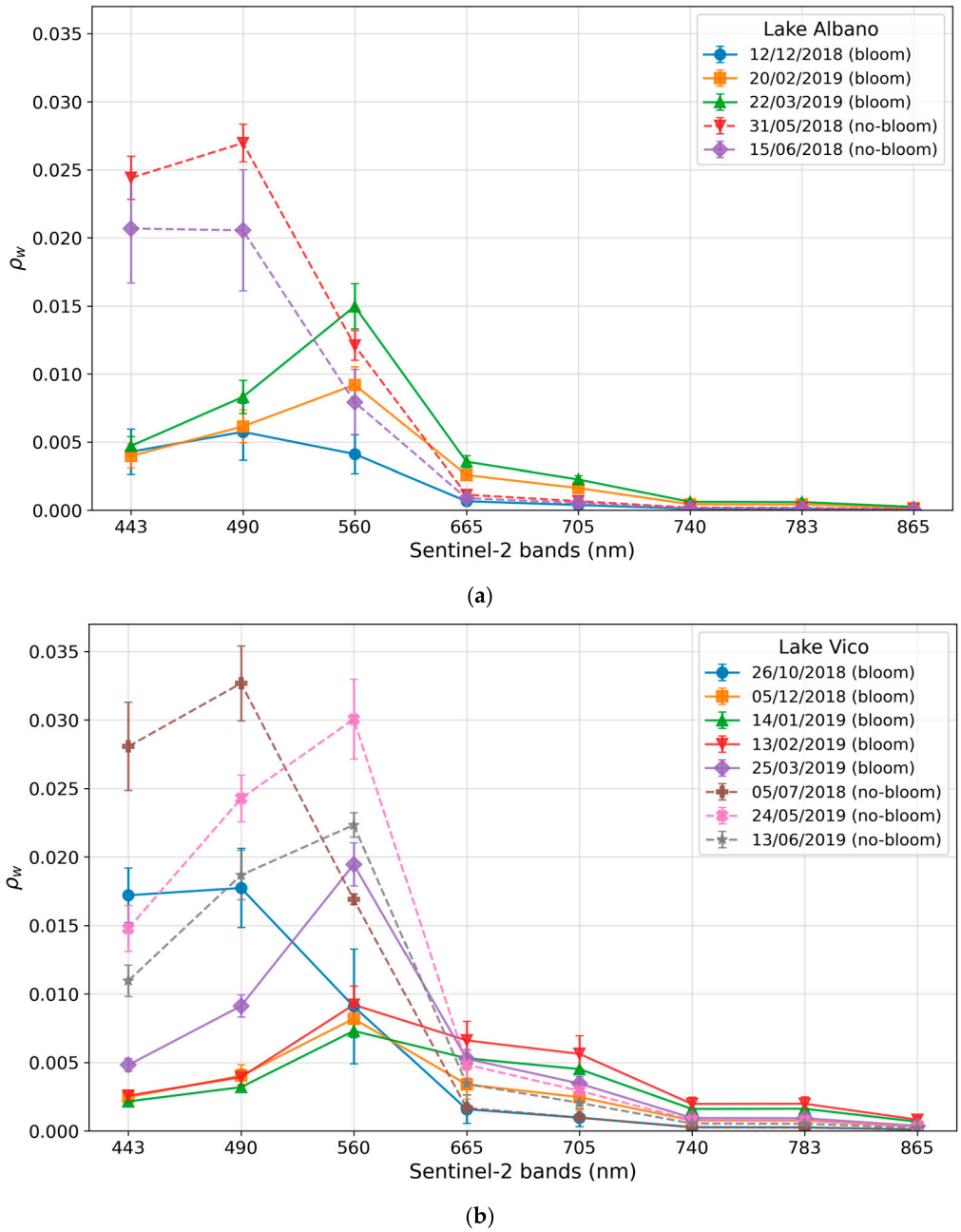

Figure 3. Mean spectral signatures of the bloom and no-bloom days under analysis, distinguished by colour and symbol according to date, for Albano (**a**) and Vico (**b**) lakes.

The graphical representation of the statistical difference between bloom and nobloom conditions, obtained through MBE, is shown in Figure 5. At the event level, MBE values appear to be strongly negative in the first two bands. There is a positive decrease in absolute magnitude in the subsequent bands, showing a comparable absolute magnitude in Bands 3, 4, and 5. The MBE becomes negligible in Bands 6 and 7, reaching 0 in Band 8A, where all spectral signatures showed a flattening. The significance, assessed through Mann–Whitney and Welch's *t*-test, showed that all the bands were significant ($p < 0.05$) under both tests (notably, Band 2 showed $p < 0.01$ with Welch's test), except for Band 3, which was significant under Mann–Whitney ($p \leq 0.047$) but not under Welch's *t*-test ($p = 0.17$).

The discrepancy in the significance between the two tests is likely to be attributable to their different nature. Because Welch's test is parametric, it is particularly sensitive to internal group variance, which is inflated for Band 3 by specific atypical bloom events, discussed below. Conversely, the Mann–Whitney U test compares the rank distribution and is therefore robust to non-normality and to atypical values in small, unequal samples. For these reasons, the non-parametric result is considered more reliable for this dataset. Additionally, the band-ratio analysis confirmed the blue-to-green ascending trend as the characteristic feature. In particular, B3/B1 drops from 3.04 in bloom conditions to 1.12 in no-bloom conditions, and B3/B2 from 1.77 to 0.76 (both $p < 0.05$), while B2/B1 has comparable values in both the conditions and low significance.

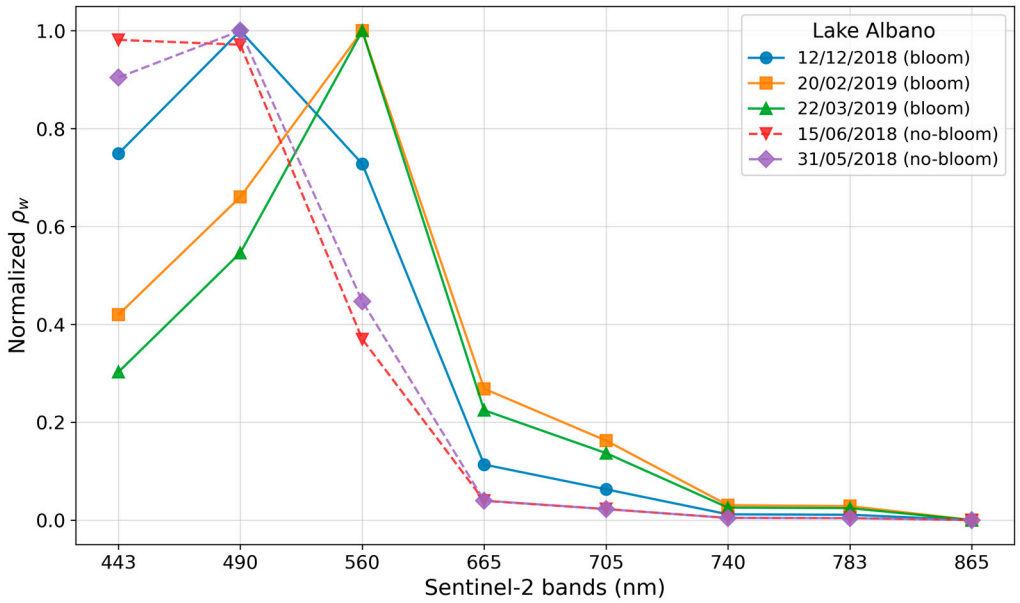

(**a**)

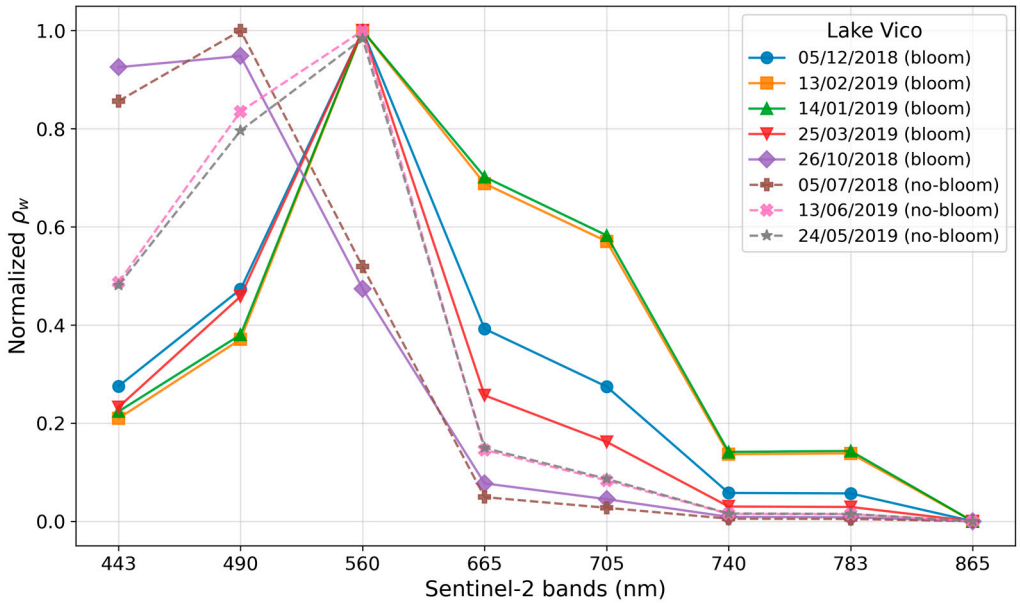

(**b**)

Figure 4. Normalized mean spectral signatures of the bloom and no-bloom days under analysis, distinguished by colour and symbol according to date, for Lake Albano (**a**) and Lake Vico (**b**).

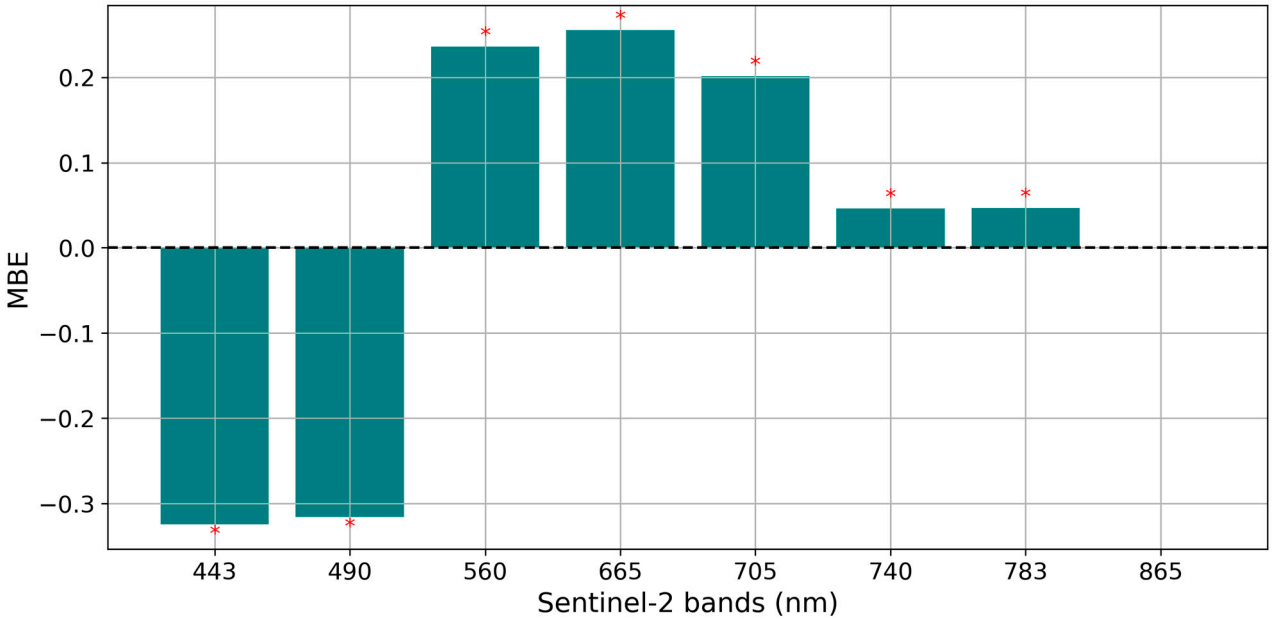

Figure 5. Bar graph exhibiting the event-level MBE for each Sentinel-2 band, between normalized spectral signatures of bloom and no-bloom days (8 bloom vs. 5 no-bloom dates). The asterisks denote Mann–Whitney significance (* $p < 0.05$).

As shown in Figure 6, the shape identified applying the classification algorithm is shared by most of the bloom signatures, with a peak in the green band and a strong increasing trend between 443 nm and 560 nm.

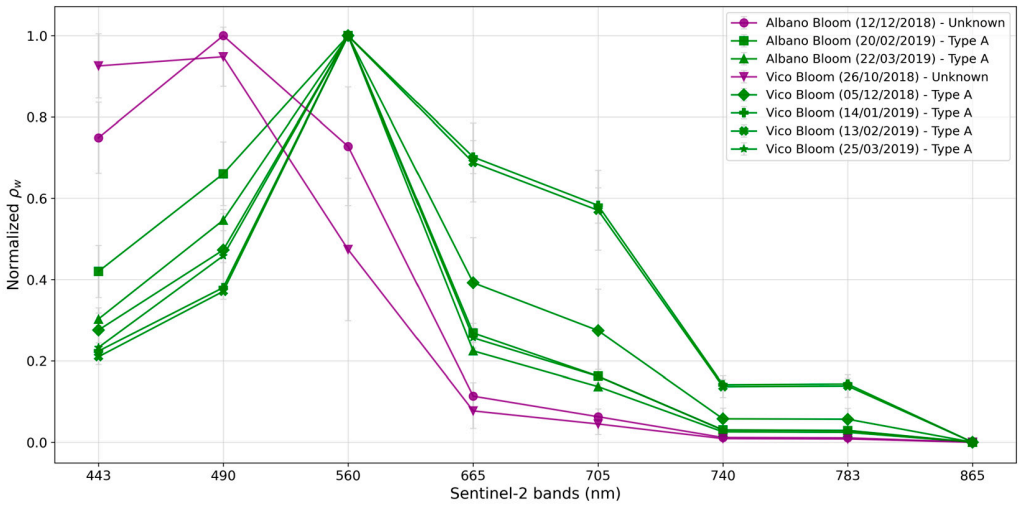

Figure 6. Normalized mean spectral signature of the bloom days. Type A signatures in green, unclassified signatures in purple.

The results of CS analysis conducted to compare the different spectral signatures of bloom events are displayed in Figure 7. More than a third of the couples compared have a cosine similarity value greater than 0.80, with 7 of the 28 combinations showing a CS between 0.96 and 1.00. Two combinations exhibit a similar negative value, and the low CS values are generally associated with the bloom event of 12 December 2018 in Albano Lake and 26 October 2018 in Vico Lake, which were already distinguishable in the spectral classification (see Figure 6).

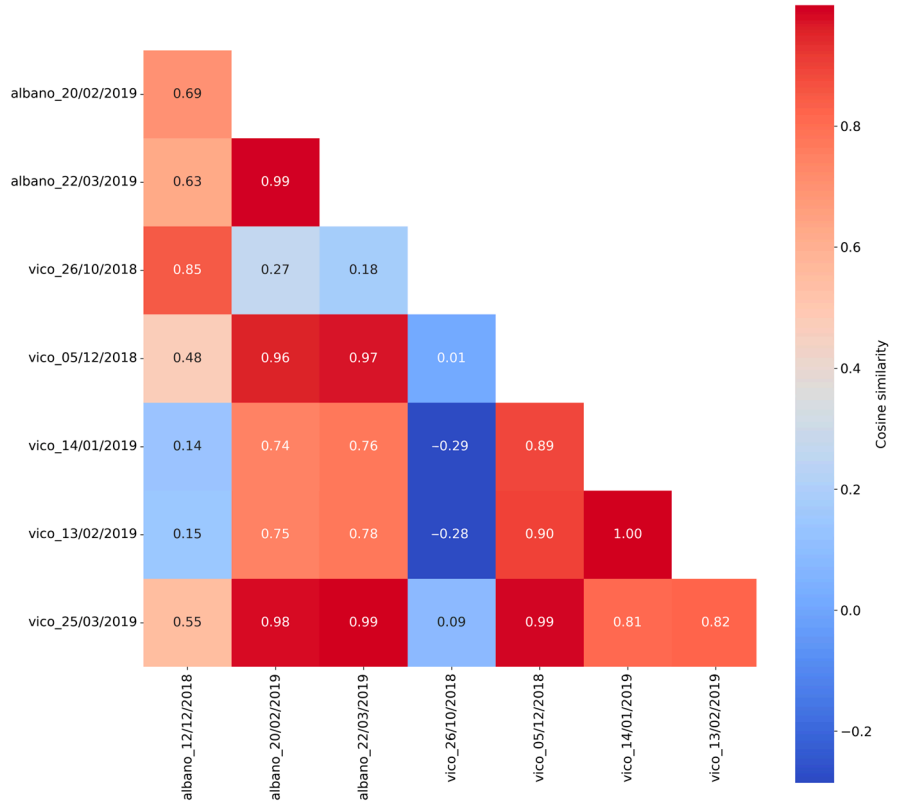

Figure 7. Heat table displaying CS values for all the combinations of coupled events. Redder values mean high cosine similarity, bluer values low similarity.

4. Discussion

This study presents a method for searching the multispectral signature pattern associated with *P. rubescens* in volcanic lakes, applied to operational satellite data (Sentinel-2/MSI imagery) and validated through in situ sampling and laboratory analyses. The samples were collected from two different volcanic basins, Vico and Albano lakes (Lazio region, Italy). Sentinel-2/MSI was selected due to its fine spatial resolution, providing eight spectral bands between 443 and 865 nm at 10 m, 20 m, or 60 m/px. The analysis highlighted that bloom conditions of *P. rubescens* were consistently distinguishable from no-bloom situations. These findings are coherent with previous studies on eutrophic lakes, where cyanobacterial blooms typically exhibit strong reflectance values in the green region [5,30]. The present work extends the previous literature aiming to contribute to an approach for defining future spectral signature catalogues as extremely useful tools for rapid and reliable detection of cyanobacterial bloom conditions.

The mean spectral signatures of each event allowed an initial distinction between bloom and no-bloom spectral response. In particular, bloom signatures generally showed lower ρ_w values, with a distinctive peak at 560 nm (green band), confirming previous observations reported by the literature [30]. Conversely, no-bloom signatures displayed higher reflectance, often with the peak at 490 nm (blue band). Both conditions shared similar behaviour from 665 nm onwards, although bloom signatures maintained relatively higher ρ_w values until 740 nm. Normalization of the signatures enabled a clearer comparison of the spectral shapes, independent of ρ_w magnitudes. Apart from two bloom events, all normalized bloom spectra showed the peak in the green band (560 nm), while the no-bloom spectra were more evenly divided between the two shapes. Even in cases where the no-bloom spectra peaked at 560 nm, they displayed comparatively higher values of ρ_w at 490 nm, resulting in a shallower trend than the bloom spectra.

These findings are in accordance with previous studies [27]. Similarly, the high values in the first two bands, observed in most of the no-bloom signatures, are also in accordance with previous studies. Higher reflectance values in Band 2, the blue band, are relatively self-evident, but higher reflectance in the first band was also expected. In this context, the wavelength 443 nm is often employed in ocean colour observation to assess the presence of suspended matter [31]. In particular, coloured dissolved organic matter (CDOM) is observed through the absorbance of this wavelength, while higher values in the reflectance of this band mean "cleaner" water.

In order to assess the difference between bloom and no-bloom spectral signatures, event-level MBE was implemented. The data showed that the normalized reflectance of the first two bands appeared to be 0.3 points lesser in the bloom signatures. Conversely, it appeared higher at almost the same magnitude in the next three bands. As shown, the p-value is significant in both the tests, except for Band 3 under Welch's test. Hence, these values confirm the statistical trustfulness of the MBE. Moreover, the band-ratio analysis confirms the ascending trend observed from Band 1 to Band 3 (the blue-to-green trend) as the distinctive trait.

Once the spectral discernibility of bloom from no-bloom conditions was established, driven by the depression of blue reflectance and a strong increasing blue-to-green trend, a soft water classification was implemented in order to synthetize the observed behaviour, implementing the waters classification approach originally proposed in 1977 [32]. Considering the nature of the observed water bodies, which can be classified as Case 2 waters [33,34], where the spectral signal may be influenced not only by phytoplankton pigments but also by suspended matter and coloured dissolved organic matter, a soft classification was implemented to highlight the common traits of the majority of the bloom signatures that had already been observed through the event-level MBE and the band-ratios. As shown in Figure 6, all but two spectral signatures (one Albano and one Vico bloom event) share the same shape (here called Type A), identified by the positive ratios between Bands 1, 2, and 3. Consequently, the Type A criterion can be seen as a compact operational synthesis of this, that is, a way to express the recurrent bloom shape as a reproducible rule. Its role is illustrative and forward-looking and its consistency across bloom events is confirmed rather than established by the subsequent CS analysis. The CS analysis was carried out between different combinations of bloom events, as shown in Figure 7. In more than half of the events, the combination produced a similarity greater than 0.70. Only in 8 of the 28 cases were the values low (between 0.27 and -0.29). In all these cases, either the bloom event of 12 December 2018 in Albano lake or that of 26 October 2018 in Vico lake was involved.

The reason behind these differences requires further investigation. In fact, such anomalous events might be interpreted as informative boundary conditions that define the limits of applicability of the identified signature. Both events occurred at seasonal transitions (late October and mid-December), when thermal stratification in Italian lakes is most sensitive to meteorological forcing [35,36]. Wind-driven mixing and cooling episodes during these periods could vertically redistribute *P. rubescens* filaments away from the surface layer sampled by the satellite, reducing the spectral signal. Therefore, these events provide a physically grounded hypothesis for future investigation; characterizing the meteorological and limnological conditions under which the "Type A" signature may not be detectable is as valuable as defining when it is. However, our results align with recent applications of Sentinel-2 imagery for algal bloom detection. In fact, a research demonstrated that indices such as the Floating Algae Index (FAI) derived from Sentinel-2 and Landsat-8 can effectively discriminate harmful algal blooms in small eutrophic lakes [37]. Similarly, another study reported a strong positive correlation between the green band and Chl-*a* concentrations in a eutrophic reservoir, confirming the key role of the

560 nm region in bloom monitoring [27]. Moreover, other works employing the Normalized Difference Chlorophyll Index (NDCI), which exploits the red-edge bands (705–740 nm), also found high accuracy in quantifying Chl-*a* in small reservoirs [38,39].

The detection of a consistent spectral signature associated with *P. rubescens* blooms suggests the feasibility of creating an operational spectral signature catalogue, which could support techniques of monitoring bloom conditions. This option has direct practical implications for the study sites themselves and beyond. With respect to the test sites chosen for this work, Vico lake supplies drinking water to approximately 10,000 residents of Ronciglione and Caprarola, while Albano lake is a major recreational resource. Thus, a 5-day revisit early-warning system based on identification of the characterized spectral pattern or other spectral patterns could trigger precautionary sampling and public health alerts before bloom conditions escalate. In practice, an operational pipeline based on this signature would involve automated flagging of Sentinel-2 acquisitions showing "Type A" spectral behaviour, followed by targeted field verification, fitting within existing water quality monitoring protocols without requiring additional instrumentation. The extension of this approach to other cyanobacterial taxa or general eutrophic conditions is beyond the scope of this study. However, the identification of a specific feature with respect to other cyanobacteria, which makes the signature specific for *P. rubescens* dominated blooms in volcanic lacustrine environment, proves the feasibility of the approach.

The dataset, limited to 13 acquisition dates across two lakes and two years, represents a deliberate proof-of-concept scope, based on the fact that the two study sites are hydrologically-independent volcanic basins with distinct morphologies, displaying bloom events that spanned multiple seasonal windows (autumn to spring). The in situ biological and toxicological produced by a national public health body associated with the Italian Health Ministry (the Italian Higher Institute of Health) ensured high-quality field and laboratory validation of the produced results. In fact, the chosen procedure is comparable to previous foundational spectral signature studies that established first-order distinguishable patterns before broader validation [14,40]. In this sense, the objective here is not to build a universal classifier, but to demonstrate the existence of a statistically consistent spectral pattern that can serve as a reference for future operational use.

A methodological consideration concerns the atmospheric correction. As previously stated, the water-leaving reflectances were retrieved with the C2RCC processor, specifically designed for optically complex (Case 2) waters, without independent in situ radiometric matching for these specific lakes. However, the focus of the proposed method is on the spectral signature relative shape (as seen in the per-spectrum normalization and spectral derivative CS analyses) and not in the absolute magnitude. As observed in a previous study, C2RCC (together with polymer processing) performed successfully in restoring the spectral shape for inland water bodies, ensuring robust retrieval [41]. This shape-based robustness is an important feature the allows transferability across water bodies and different sites. However, we acknowledge that a full radiometric validation of C2RCC over these volcanic basins remains to be performed and dedicated match-up campaigns would certainly strengthen the reliability of the retrieved reflectances.

Finally, several limitations must be acknowledged. First, the temporal coverage of bloom events was limited, preventing the construction of a more robust catalogue across multiple years. Second, the analysis was restricted to two Italian volcanic basins, which limits the extension of the findings to other lake types. Third, Sentinel-2/MSI, while effective and able to observe with an extremely high resolution, cannot capture the finer spectral details available from hyperspectral sensors, which could further improve discrimination of different bloom types. Future research should extend the analysis to a broader set of lakes and bloom events; moreover, upcoming hyperspectral missions could

also provide valuable insights to refine the detection of cyanobacterial blooms at higher spectral resolution.

5. Conclusions

This study underscores the potential of integrating remote and proximal sensing technologies for the detection and monitoring of *P. rubescens*, a cyanobacterium associated with increasing ecological and health concerns. By leveraging spectral signature analysis, this research addresses critical gaps in the remote sensing of HABs. It adopts a spectral signature approach to support the detection of HAB conditions, offering a robust methodology for observing and locating water bodies affected by cyanobacteria. The development of a multispectral reference pattern, specifically tailored for operational sensors like Sentinel-2, represents an important complementary method for improving the precision and reliability of monitoring tools for aquatic ecosystems. This spectral signature approach offers an adaptable and repeatable methodology across different environments, providing a practical solution for the ongoing challenges posed by HABs.

Data collected from two Italian lakes, Albano and Vico, illustrate the applicability and versatility of this method across different water bodies. The study, despite having to depend on a limited number of events, reveals that Albano and Vico Lakes exhibited strong similarities in their spectral signature shapes when satellite data from blooms were observed. These results suggest that *P. rubescens* blooms produce a recognizable spectral signature, at least in the volcanic lakes studied. This pattern, distinct from no-bloom conditions, provides a basis for developing automated detection algorithms applicable to similar water bodies.

One of the key contributions of this research lies in demonstrating the potential of multispectral data, combined with historical in situ observations, to observe a common spectral signature that increases the capability to discriminate *P. rubescens* blooms under specific conditions. The findings also demonstrate that the proposed methodology can significantly improve the temporal and spatial coverage of bloom detection, particularly compared to in situ sampling alone. By facilitating the integration of remote sensing data with in-situ measurements, this approach supports the development of advanced early warning systems for bloom identification. Looking ahead, future research will aim to solidify these findings by employing data from additional satellite archives and analyzing a broader range of water bodies. This will help establish a more comprehensive database of distinguishable reference signatures for use in new investigations.

Coupling these investigations with specific environmental and limnological analyses in future works can help relate the observed spectral patterns to bloom drivers, deepen our understanding of the ecological factors behind HABs, enabling more precise and effective monitoring efforts. To further enhance this approach, the integration of remote sensing and proximal sensing technologies, such as drones with multi/hyperspectral cameras, will be sought to improve data collection capabilities. Merging these techniques with in situ observations to implement a multi-layered approach will enhance spatio-temporal resolution, ultimately leading to more accurate management techniques for HABs. Additionally, machine learning techniques that merge situational awareness frameworks and probabilistic forecasting models will be further explored. The continued development of spectral signature libraries, combined with multi-source monitoring frameworks, offers a promising path forward for mitigating the impacts of HABs on ecosystems and human communities alike.

Author Contributions: Conceptualization, C.C., M.A., M.B., V.M. and M.L.; Methodology, C.C., M.A., M.B., V.M. and M.L.; Software, C.C., M.A. and M.L.; Formal Analysis, C.C., M.A. and M.L.; Investigation, C.C., M.A. and M.L.; Data Curation, C.C., M.A. and M.L.; Validation, C.C., M.A., M.B.,

V.M. and M.L.; Resources, M.L.; Supervision, M.C. and M.L.; Writing—Original Draft Preparation, C.C., M.A., M.B. and V.M.; Writing—Review and Editing, C.C., M.A., M.C. and M.L. All authors have read and agreed to the published version of the manuscript.

Funding: This research received no external funding.

Data Availability Statement: Sentinel-2 satellite data employed for the analyses of this study are publicly available from the Copernicus Data Space Ecosystem https://dataspace.copernicus.eu (accessed on 1 June 2025) and were processed using the ESA SNAP v13.0 software. In situ data were collected and analyzed by the authors and are not publicly available.

Acknowledgments: Some authors conducted the activities described here within the framework of the international PhD program and the UNESCO Chair 'Environment, Resources and Sustainable Development', thanks also to the Italian Aerospace Research Centre (CIRA). The authors' activities were also supported by the line of research of Massimiliano Lega and Situational Awareness for Environment (SAfE) team.

Conflicts of Interest: The authors declare no conflicts of interest.

References

1. Huisman, J.; Codd, G.A.; Paerl, H.W.; Ibelings, B.W.; Verspagen, J.M.H.; Visser, P.M. Cyanobacterial Blooms. *Nat. Rev. Microbiol.* **2018**, *16*, 471–483. [CrossRef] [PubMed]
2. Villalobos, T.; Suárez-Isla, B.; Garcia, C. Health and Environmental Impacts of Cyanobacteria and Cyanotoxins from Freshwater to Seawater. *Toxins* **2025**, *17*, 126. [CrossRef] [PubMed]
3. Lega, M.; Casazza, M.; Teta, R.; Zappa, C.J. Environmental Impact Assessment: A Multilevel, Multi-Parametric Framework for Coastal Waters. *Int. J. SDP* **2018**, *13*, 1041–1049. [CrossRef]
4. Borges, H.D.; Cicerelli, R.E.; De Almeida, T.; Roig, H.L.; Olivetti, D. Monitoring Cyanobacteria Occurrence in Freshwater Reservoirs Using Semi-Analytical Algorithms and Orbital Remote Sensing. *Mar. Freshw. Res.* **2020**, *71*, 569–578. [CrossRef]
5. Wang, J.; Wang, Z.; Cui, Y.; Yan, S. Dynamic Monitoring of Phycocyanin Concentration in Chaohu Lake of China Using Sentinel-3 Images and Its Indication of Cyanobacterial Blooms. *Ecol. Indic.* **2022**, *143*, 109340. [CrossRef]
6. Liu, H.; Li, Q.; Shi, T.; Hu, S.; Wu, G.; Zhou, Q. Application of Sentinel 2 MSI Images to Retrieve Suspended Particulate Matter Concentrations in Poyang Lake. *Remote Sens.* **2017**, *9*, 761. [CrossRef]
7. Pahlevan, N.; Sarkar, S.; Franz, B.A.; Balasubramanian, S.V.; He, J. Sentinel-2 MultiSpectral Instrument (MSI) Data Processing for Aquatic Science Applications: Demonstrations and Validations. *Remote Sens. Environ.* **2017**, *201*, 47–56. [CrossRef]
8. Karetnikov, S.; Leppäranta, M.; Montonen, A. A Time Series of over 100 Years of Ice Seasons on Lake Ladoga. *J. Gt. Lakes Res.* **2017**, *43*, 979–988. [CrossRef]
9. Selmeczy, G.B.; Costa, M.; Padisák, J.; Vasas, G. Biogeography, Life Strategy and Ecology of Planktothrix Rubescens: A Review. *Hydrobiologia* **2025**, *852*, 3231–3256. [CrossRef]
10. Knapp, D.; Fernández Castro, B.; Marty, D.; Loher, E.; Köster, O.; Wüest, A.; Posch, T. The Red Harmful Plague in Times of Climate Change: Blooms of the Cyanobacterium Planktothrix Rubescens Triggered by Stratification Dynamics and Irradiance. *Front. Microbiol.* **2021**, *12*, 705914. [CrossRef] [PubMed]
11. Boscaini, A.; Brescancin, F.; Cerasino, L.; Fedrigotti, C.; Fano, E.A.; Salmaso, N. Vertical and Horizontal Distribution of the Microcystin Producer Planktothrix Rubescens (Cyanobacteria) in a Small Perialpine Reservoir. *Adv. Ocean. Limnol.* **2017**, *8*. [CrossRef]
12. Messineo, V.; Mattei, D.; Melchiorre, S.; Salvatore, G.; Bogialli, S.; Salzano, R.; Mazza, R.; Capelli, G.; Bruno, M. Microcystin diversity in a Planktothrix rubescens population from Lake Albano (Central Italy). *Toxicon* **2006**, *48*, 160–174. [CrossRef]
13. Cannicci, G. Su Una Eccezionale Fioritura Del Lago Di Albano. *Boll. Pesca Piscic. Idrobiol.* **1953**, *8*, 221–233.
14. Copetti, D.; Matarrese, R.; Bresciani, M.; Guzzella, L. Integration of In Situ and Remote Sensing Measurements for the Management of Harmful Cyanobacteria Blooms. A Lesson from a Strategic Multiple-Uses Reservoir (Lake Occhito, South Italy). *Water* **2021**, *13*, 2162. [CrossRef]
15. Kim Tiam, S.; Comte, K.; Dalle, C.; Delagrange, M.; Djediat, C.; Ducos, B.; Duval, C.; Feilke, K.; Hamlaoui, S.; Le Manach, S.; et al. The Success of the Bloom-Forming Cyanobacteria Planktothrix: Genotypes Variability Supports Variable Responses to Light and Temperature Stress. *Harmful Algae* **2022**, *117*, 102285. [CrossRef] [PubMed]
16. Laneve, G.; Téllez, A.; Kallikkattil Kuruvila, A.; Bruno, M.; Messineo, V. Eutrophication and HAB Occurrence Control in Lakes of Different Origins: A Multi-Source Remote Sensing Detection Strategy. *Remote Sens.* **2024**, *16*, 1792. [CrossRef]

17. Legleiter, C.J.; King, T.V.; Carpenter, K.D.; Hall, N.C.; Mumford, A.C.; Slonecker, T.; Graham, J.L.; Stengel, V.G.; Simon, N.; Rosen, B.H. Spectral Mixture Analysis for Surveillance of Harmful Algal Blooms (SMASH): A Field-, Laboratory-, and Satellite-Based Approach to Identifying Cyanobacteria Genera from Remotely Sensed Data. *Remote Sens. Environ.* **2022**, *279*, 113089. [CrossRef]
18. Fournier, C.; Quesada, A.; Cirés, S.; Saberioon, M. Discriminating Bloom-Forming Cyanobacteria Using Lab-Based Hyperspectral Imagery and Machine Learning: Validation with Toxic Species under Environmental Ranges. *Sci. Total Environ.* **2024**, *932*, 172741. [CrossRef] [PubMed]
19. Bruno, M.; Messineo, V.; Mattei, D.; Melchiorre, D. *Dinamica Di Specie Algali Tossiche Nei Laghi Di Albano e Nemi*; Rapporti ISTISAN; Istituto Superiore di Sanità: Roma, Italy, 2004.
20. Utermöhl, H. Neue Wege in der quantitativen Erfassung des Plankton. (Mit besonderer Berücksichtigung des Ultraplanktons.): Mit 4 Abbildungen im Text. *Int. Ver. Theor. Angew. Limnol. Verhandlungen* **1931**, *5*, 567–596. [CrossRef]
21. Lund, J.W.G.; Kipling, C.; Le Cren, E.D. The Inverted Microscope Method of Estimating Algal Numbers and the Statistical Basis of Estimations by Counting. *Hydrobiologia* **1958**, *11*, 143–170. [CrossRef]
22. Aminot, A.; Rey, F. Chlorophyll a: Determination by Spectroscopic Methods. *ICES Tech. Mar. Environ. Sci.* **2001**. [CrossRef]
23. Shamloo, A.; Sima, S. Investigating the Potential of Remote Sensing-Based Machine-Learning Algorithms to Model Secchi-Disk Depth, Total Phosphorus, and Chlorophyll-a in Lake Urmia. *J. Gt. Lakes Res.* **2024**, *50*, 102370. [CrossRef]
24. Schaeffer, B.A.; Reynolds, N.; Ferriby, H.; Salls, W.; Smith, D.; Johnston, J.M.; Myer, M. Forecasting Freshwater Cyanobacterial Harmful Algal Blooms for Sentinel-3 Satellite Resolved U.S. Lakes and Reservoirs. *J. Environ. Manag.* **2024**, *349*, 119518. [CrossRef] [PubMed]
25. Binding, C.E.; Zastepa, A.; Zeng, C. The Impact of Phytoplankton Community Composition on Optical Properties and Satellite Observations of the 2017 Western Lake Erie Algal Bloom. *J. Gt. Lakes Res.* **2019**, *45*, 573–586. [CrossRef]
26. Zheng, W.; Chen, L.; Chen, R.; Li, M.; Bao, Q.; Liu, H.; Tang, X. Spatiotemporal Variation and Key Environmental Drivers of Chlorophyll-a in Qionghai Lake: Insights from Sentinel-2 Satellite and Machine Learning Models. *Discov. Sustain.* **2025**, *7*, 174. [CrossRef]
27. Viso-Vázquez, M.; Acuña-Alonso, C.; Rodríguez, J.L.; Álvarez, X. Remote Detection of Cyanobacterial Blooms and Chlorophyll-a Analysis in a Eutrophic Reservoir Using Sentinel-2. *Sustainability* **2021**, *13*, 8570. [CrossRef]
28. Chen, B.; Chen, Y.; Chen, H. An Interpretable CatBoost Model Guided by Spectral Morphological Features for the Inversion of Coastal Water Quality Parameters. *Water* **2024**, *16*, 3615. [CrossRef]
29. Irimatsugawa, T.; Shimizu, Y.; Okubo, S.; Inaba, H. Cosine Similarity for Quantitatively Evaluating the Degree of Change in an Optical Frequency Comb Spectra. *Opt. Express* **2021**, *29*, 35613. [CrossRef] [PubMed]
30. Song, T.; Liu, G.; Zhang, H.; Yan, F.; Fu, Y.; Zhang, J. Lake Cyanobacterial Bloom Color Recognition and Spatiotemporal Monitoring with Google Earth Engine and the Forel-Ule Index. *Remote Sens.* **2023**, *15*, 3541. [CrossRef]
31. Zhang, Y.; Van Dijk, M.A.; Liu, M.; Zhu, G.; Qin, B. The Contribution of Phytoplankton Degradation to Chromophoric Dissolved Organic Matter (CDOM) in Eutrophic Shallow Lakes: Field and Experimental Evidence. *Water Res.* **2009**, *43*, 4685–4697. [CrossRef] [PubMed]
32. Morel, A.; Prieur, L. Analysis of Variations in Ocean Color. *Limnol. Oceanogr.* **1977**, *22*, 709–722. [CrossRef]
33. Perrone, M.; Scalici, M.; Conti, L.; Moravec, D.; Kropáček, J.; Sighicelli, M.; Lecce, F.; Malavasi, M. Water Mixing Conditions Influence Sentinel-2 Monitoring of Chlorophyll Content in Monomictic Lakes. *Remote Sens.* **2021**, *13*, 2699. [CrossRef]
34. Neil, C.; Spyrakos, E.; Hunter, P.D.; Tyler, A.N. A Global Approach for Chlorophyll-a Retrieval across Optically Complex Inland Waters Based on Optical Water Types. *Remote Sens. Environ.* **2019**, *229*, 159–178. [CrossRef]
35. Rogora, M.; Buzzi, F.; Dresti, C.; Leoni, B.; Lepori, F.; Mosello, R.; Patelli, M.; Salmaso, N. Climatic Effects on Vertical Mixing and Deep-Water Oxygen Content in the Subalpine Lakes in Italy. *Hydrobiologia* **2018**, *824*, 33–50. [CrossRef]
36. Woolway, R.I.; Sharma, S.; Weyhenmeyer, G.A.; Debolskiy, A.; Golub, M.; Mercado-Bettín, D.; Perroud, M.; Stepanenko, V.; Tan, Z.; Grant, L.; et al. Phenological Shifts in Lake Stratification under Climate Change. *Nat. Commun.* **2021**, *12*, 318. [CrossRef] [PubMed]
37. Liu, M.; Ling, H.; Wu, D.; Su, X.; Cao, Z. Sentinel-2 and Landsat-8 Observations for Harmful Algae Blooms in a Small Eutrophic Lake. *Remote Sens.* **2021**, *13*, 4479. [CrossRef]
38. Zolfaghari, K.; Pahlevan, N.; Binding, C.; Gurlin, D.; Simis, S.G.H.; Verdú, A.R.; Li, L.; Crawford, C.J.; Vanderwoude, A.; Errera, R.; et al. Impact of Spectral Resolution on Quantifying Cyanobacteria in Lakes and Reservoirs: A Machine-Learning Assessment. *IEEE Trans. Geosci. Remote Sens.* **2022**, *60*, 5515520. [CrossRef]
39. Kislik, C.; Dronova, I.; Grantham, T.E.; Kelly, M. Mapping Algal Bloom Dynamics in Small Reservoirs Using Sentinel-2 Imagery in Google Earth Engine. *Ecol. Indic.* **2022**, *140*, 109041. [CrossRef]

40. Vareli, K.; Briasoulis, E.; Pilidis, G.; Sainis, I. Molecular Confirmation of Planktothrix Rubescens as the Cause of Intense, Microcystin—Synthesizing Cyanobacterial Bloom in Lake Ziros, Greece. *Harmful Algae* **2009**, *8*, 447–453. [CrossRef]
41. Warren, M.A.; Simis, S.G.H.; Martinez-Vicente, V.; Poser, K.; Bresciani, M.; Alikas, K.; Spyrakos, E.; Giardino, C.; Ansper, A. Assessment of Atmospheric Correction Algorithms for the Sentinel-2A MultiSpectral Imager over Coastal and Inland Waters. *Remote Sens. Environ.* **2019**, *225*, 267–289. [CrossRef]

Disclaimer/Publisher's Note: The statements, opinions and data contained in all publications are solely those of the individual author(s) and contributor(s) and not of MDPI and/or the editor(s). MDPI and/or the editor(s) disclaim responsibility for any injury to people or property resulting from any ideas, methods, instructions or products referred to in the content.